Terrain Modeling in Synthetic Aperture Radar Images using Shape-from-Shading

Adrian G. Bors, Edwin R. Hancock and Richard C. Wilson

Department of Computer Science, University of York, York YO10 5DD, U.K.

Abstract

In this paper we introduce a new approach for recovering shape-from-shading (SFS) from synthetic aperture radar (SAR) images of the terrain. Three contributions are proposed. Firstly, we show how the direction of surface normals is constrained by the geometry of the radar reflectivity cone. Second, we show how topographic features can be used as boundary constraints on the recovered surface normals. Finally, the resulting field of surface normals is smoothed using robust statistics.

1 Introduction

Radar shape-from-shading has proved to be an alluring, yet somewhat elusive tool for probing the three dimensional structure of the terrain. Shape-from-shading has been used in computer vision to extract surface height and orientation information from Lambertian objects by solving image irradiance equation [1]. The problem is invariably couched in a variational framework, where data-closeness and smoothness penalties are minimized subject to constraints imposed by boundary conditions. One of the criticisms of this classical approach is the poor data-closeness with the image irradiance equation and the resultant over smoothing of the recovered surface information. This deficiency has recently been addressed by Worthington and Hancock [2] who provide a simple geometric method which precisely satisfies the image irradiance equation as a hard constraint.

The aim in this paper is to investigate whether this method can be extended to the radar domain, where Lambertian reflectance models no longer apply. There have been several attempts at using SFS for recovering terrain topography from synthetic aperture radar imagery [3, 4]. In SAR images, the simple and convenient Lambertian reflectance model is no longer applicable [3]. To extend the geometric framework from [2], we therefore commence by modeling the SAR reflectance function using ground truth information provided by a digital elevation map. Using the empirical reflectance function we develop a geometric method for solving the SAR reflectivity equation. This allows us to estimate the terrain surface orientation provided that boundary constraints and smoothness constraints are available. The boundary constraints are provided by the estimated locations of salient terrain features such as ridges and ravines. The surface smoothness constraints are furnished by median statistics. The new radar shape-from-shading method is validated on SAR terrain images.

2 SAR reflectivity function

In the case of SAR images, the Lambertian assumption does not hold [3, 4] and it is necessary to provide a more complex model for the reflectance function. In such images, the illumination is directed along the tilt axis, so the radar irradiance function is :

$$I(r,a) = \mathcal{R}\left(\frac{\cos\alpha - p\sin\alpha}{\sqrt{1+p^2+q^2}}\right) \tag{1}$$

where α is the angle between the illumination direction and the z axis, while p, q are the partial derivatives of the height with respect to the range and azimuth denoted as r and a.

We can estimate the reflectivity model if we have access to a digital elevation map (DEM) for a given SAR image. An example of a SAR image for a mountainous region in Wales is shown in Figure 1a. This image corresponds to a nominal antenna depression angle $\alpha = 20$ degrees. The features of terrain are not visible in this image due to the nonlinear characteristics of the reflectance function. Its corresponding DEM is shown in Figure 1b. Empirically, using the association between the images from Figures 1a and 1b we have found that the inverse of the reflectivity function can be approximated by the following function :

$$\mathbf{N}^T\mathbf{L} = \cos\gamma = \mathcal{R}^{-1}(I(r,a)) = \frac{I(r,a) - 55}{0.8I(r,a)} \tag{2}$$

where γ is the angle between the illumination direction $\mathbf{L}$ and the surface normal $\mathbf{N}$. In Figure 2a, the proposed model from (2) is represented with continuous line, while the experimental data is shown with a dotted line. Figure 1c shows the result of applying the inverse reflectivity function displayed in Figure 2a to the radar image shown in Figure 1a.

0-7695-0750-6/00 $10.00 © 2000 IEEE

We can clearly observe in this image a much better contrast, while terrain structures become identifiable. We have investigated alternative empirical models for the reflectance function, including piecewise polynomials. The fitting of a piecewise polynomial function to the inverse of the reflectivity function is displayed in Figure 2b, while the recovery of the radar image from Figure 1a, using a piecewise polynomial approximation, is shown in Figure 1d. Due to its property of being continuous on the entire interval of interest, we choose to use the formula (2) for approximating the inverse of the reflectance function.

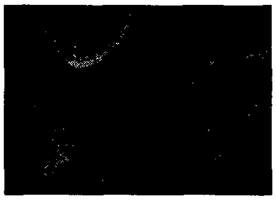

(a) Original SAR image

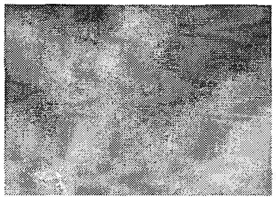

(b) Digital elevation map

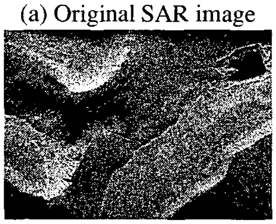

(c) SAR image recovery using (2)

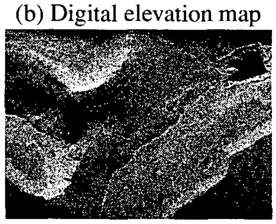

(d) SAR image recovery using a polynomial approx.

Figure 1. SAR image recovery.

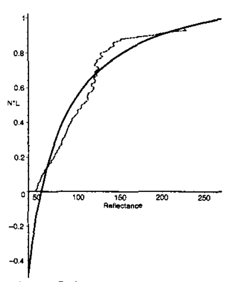

(a) Using (2)

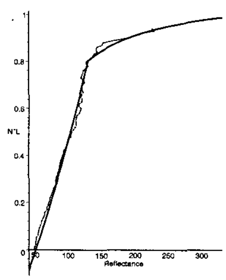

(b) Using a polynomial approximation

Figure 2. Modeling the reflectance function.

The shape-from-shading process requires boundary constraints for surface normal orientation at certain key image locations [1, 2]. In the case of terrain images we can use the ridges and ravines as boundary constraints. Such features generally correspond to edges in SAR images. We can show that a SAR image is characterized by the following probability density function [5] :

$$p(x) = \frac{x}{\pi\sigma^2} \exp\left[-\frac{x^2+\mu^2}{2\sigma^2}\right] \int_0^\pi \exp\left[\frac{x\mu}{\sigma^2}\cos\theta\right] d\theta$$

$$= \frac{x}{\sigma^2} \exp\left[-\frac{x^2+\mu^2}{2\sigma^2}\right] I_0\left(\frac{x\mu}{\sigma^2}\right) \quad (3)$$

where $I_0(x\mu/\sigma^2)$ is a modified Bessel function. This distribution function is a product of two terms : one models the uncorrelated noise component while the other one models the correlation of the complex radar signal due to interference. After estimating its parameters we can derive a maximum log-likelihood estimator. We classify the terrain features by comparing the value of the image amplitude in the range direction on the either side of an edge. The ridge side facing the illumination source is more intensely illuminated than the other side, while ravines are characterized by the opposite behavior.

3 Shape from Shading in SAR images

In [1] a variational framework for shape-from-shading was proposed. There is a data-closeness term which models compliance with the image irradiance equation and a smoothing term which regularises the recovered needle map. Both concave and convex surfaces produce the same variation in the shading. For solving this ambiguity we consider edge constraints in the energy expression from [1]. Ravines are used as attractors, while ridges are difractors for the surface normals. The expression of the energy function in the new context is given by :

$$E = \sum_{a=1}^{M-1}\sum_{r=1}^{P-1}\{[\mathcal{R}^{-1}(I(r,a)) - \mathbf{N}_{r,a}^T\mathbf{L}] + \lambda_1 \sum_{i=a-1}^{a+1}\sum_{j=r-1}^{r+1} ||\mathbf{N}_{r,a} - \mathbf{N}_{i,j}|| \pm \lambda_2\mathbf{N}_{r,a}^T\mathbf{E}_{k,l}\} \quad (4)$$

where $\mathcal{R}^{-1}$ is the inverse of the reflectance function, derived in (2), $\mathbf{N}_{r,a}$ is the surface normal at location (r, a), $\mathbf{L}$ is the light source direction, $\mathbf{E}_{k,l}$ is the orientation of the nearest edge, $M \times P$ is the image size and $\lambda_{1,2}$ are weighting factors for the energy components. The second part of this expression corresponds to smoothing the vector field on a 3×3 neighborhood. The third part of the energy function corresponds to boundary constraints. Minimizing this energy results in vectors which are perpendicular on the closest edge; the normal vector points towards a ravine and points in the opposite direction of a ridge. Shadow regions as well as water correspond to a very low reflectivity, and they are not well modeled by the reflectance function. Water is characterized by the lowest range of values for the interference parameter μ from (3). Since the surface of water is horizontal, the associated surface normals are parallel with z axis. Shadow regions correspond to back slopes and they are characterized by intermediate values of μ. Such regions correspond to orientation angles of $\gamma > \frac{\pi}{2}$.

In [2], the Horn and Brooks approach has been rendered more robust by considering the irradiance equation as a hard constraint. According to that approach, the surface normals must always lie on the surface of a cone. In the case of SAR images there is an uncertainty in the estimation of the angle

γ due to the SAR signal variance, σ^2. We use the standard deviation to define the following interval for the apex angle of the cone :

$$\cos(\gamma) \in \left[\mathbf{N}^T\mathbf{L} - \frac{\hat{\sigma}}{4}, \mathbf{N}^T\mathbf{L} + \frac{\hat{\sigma}}{4}\right] \quad (5)$$

The range of possible values for the surface normal is shown in Figure 3.

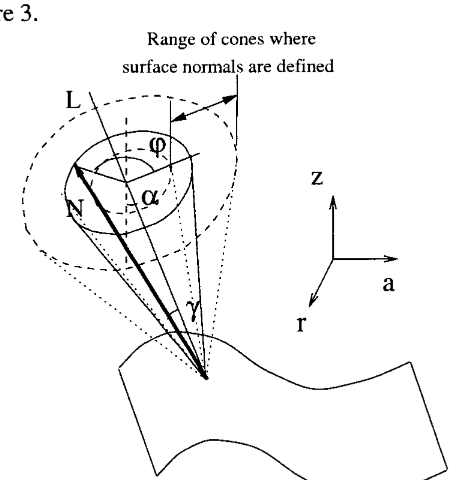

Figure 3. Surface normal orientation.

We have shown how to estimate the opening angle of the radar reflectance cone γ and the direction of the surface normal ϕ. We can use these angles to estimate the direction of the surface normal. In the case of SAR images, the azimuthal angle of the radar beam is $\pi/2$, while the inclination angle with the (z, a) plane is denoted by α. The surface normal is given in rectangular coordinates by :

$$\begin{aligned} N_r &= \sin\gamma\sin\phi\cos\alpha + \cos\gamma\sin\alpha \\ N_a &= \sin\gamma\cos\phi \\ N_h &= -\sin\gamma\sin\phi\sin\alpha + \cos\gamma\cos\alpha \end{aligned} \quad (6)$$

4 Normal vector field smoothing

In this Section we show how we minimize the second energy component from (4). One way to minimize the energy is to apply adaptive local averaging as in [1]. At iteration $t+1$, the updated surface normals are given by :

$$\hat{\mathbf{N}}_j(t+1) = \hat{\mathbf{N}}_j(t) - \varepsilon\left[\hat{\mathbf{N}}_j(t) - \frac{\sum_l \hat{\mathbf{N}}_l(t)}{n^2-1}\right] \quad (7)$$

where $\varepsilon \in (0,1)$ is the updating rate and (i,j) are sites from the neighborhood of (r,a), $(i,j) \in \mathcal{N}(r,a)$, which is considered to be of size $n \times n$.

By using this smoothing rule, the borders between various objects are smeared [2]. We consider two alternative updating rules based on robust statistics. The first of these, employs the marginal median :

$$\hat{\mathbf{N}}_j(t+1) = \mathrm{med}\{\hat{\mathbf{N}}_l(t), l \in \mathcal{N}_j\} \quad (8)$$

where the median estimator is applied on each component of the surface normal, separately. The second robust estimator is the vector median [6]. This estimator chooses the vector which has the smallest distance to all the other vectors from the given neighborhood :

$$\hat{\mathbf{N}}_j(t+1) = \hat{\mathbf{N}}_l(t), \quad l = \arg\min_k \sum_{i\in\mathcal{N}_j} ||\hat{\mathbf{N}}_k - \hat{\mathbf{N}}_i|| \quad (9)$$

where $k \in \mathcal{N}_j$.

After updating the surface normals, we backproject them onto one of the radar reflectance cones as defined in Figure 3. We constrain the vector normals to lie into the interval defined in (5) at any time in the iterative smoothing process. The shape-from-shading algorithm iterates to minimize the energy function (4) while maintaining the constraints from (5).

5 Experimental results

We have used the proposed algorithm to SAR images of mountainous terrain. After applying the inverse reflectivity function which has been derived in Section 2, we split the image in blocks of 20×20 pixels and we estimate the parameters of the Rayleigh-Bessel distribution (3) in each of them. We estimate the edges using the maximum log-likelihood estimator for the Rayleigh-Bessel distribution. We use the edge map as constraints for the vector field. We employ the iterative approach described in Section 4 for smoothing the vector field. In the first stage the surface normals are smoothed. In the second stage, the consistency of the vector normals with the image statistics is verified according to (5). If the normal vector corresponds to a parameter range which is outside the range provided by the SAR image local statistics, as given by (5), their values are corrected accordingly.

The vector field smoothed by marginal median is shown in Figure 4, while the vector field smoothed by the vector median and by the surface consistency using the shape index described in [2] are displayed in Figures 5 and 6, respectively. The neighborhood used in all these experiments is 3×3 vectors. We can observe in these images that the vector field is quite well smoothed. We consider the surface normal vector field of the digital elevation map from Figure 1b as a reference vector field. The mean square error (MSE) and the mean cosine error (MCE) for the angle between the reference and the smoothed surface normal vector field, when smoothing is performed by using averaging (7), marginal median (8), vector median (9) and surface consistency is provided in Table 1. If the reference and smoothed normal vectors would have the same orientation, then the cosine of their angle would be 1. From Table 1 we see that robust estimators provide better shape modeling capabilities, and smoothing is achieved in fewer iterations then by using local averaging.

Table 1. Smoothing algorithms evaluation

Algorithm	MSE	MCE	No. Iterations
Averaging	0.824	0.551	199
Marginal Median	0.816	0.553	88
Vector Median	0.797	0.567	42
Curvature Consistency	0.821	0.553	13

6 Conclusions

We have proposed a new approach for shape from shading in SAR images. The SAR amplitude is considered to be distributed according to the Rayleigh-Bessel distribution. We detect main terrain features in the SAR image and we classify them according to the image statistics. We derive a SFS model to be applied for SAR images representing terrain. The 3-D shape is represented as a vector field of local normals. We employ local smoothing of the normal vector field. The results obtained show that main terrain components as mountains, valleys and lakes are quite well defined. The proposed algorithms are suitable for terrain modeling and topographical feature identification.

References

[1] B. K. P. Horn, M. J. Brooks, "The variational approach to shape from shading," *Computer Vision, Graphics, Image Processing*, vol. 33, no. 2, 1986, pp. 174-208.

[2] P. L. Worthington, E. R. Hancock, "New constraints on data-closeness and needle map consistency for shape-from-shading," *IEEE Trans. on Pattern Analysis and Machine Intelligence*, vol. 21, no. 12, pp. 1250-1267, 1999.

[3] R. T. Frankot, R. Chellappa, "Estimation of surface topography from SAR imagery using shape from shading techniques," *Artificial Intelligence*, vol. 43, pp. 270-310, 1990.

[4] P. Fua, "Fast, accurate and consistent modeling of drainage and surrounding terrain," *Inter. J. of Computer Vision*, vol. 26, no. 3, pp. 215-234, 1998.

[5] A. Papoulis, *Probability, Random variables and Stochastic Processes.* McGraw-Hill, 1984.

[6] J. Astola, P. Haavisto, Y. Neuvo, "Vector median filters," *Proc. of IEEE*, vol. 78, no. 4, pp. 678-689, 1990.

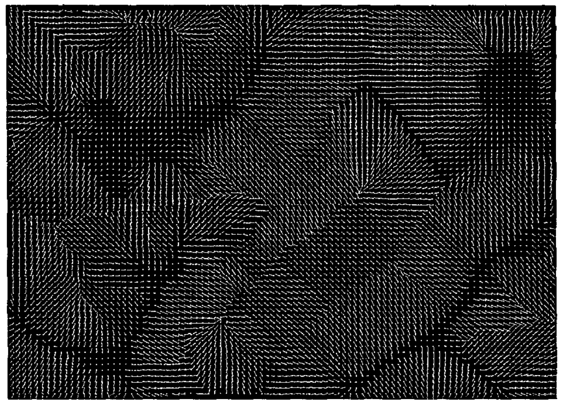

Figure 4. Surface normals smoothed by the marginal median.

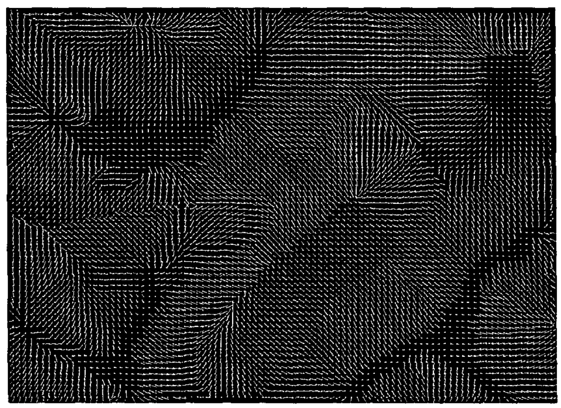

Figure 5. Surface normals smoothed by the vector median.

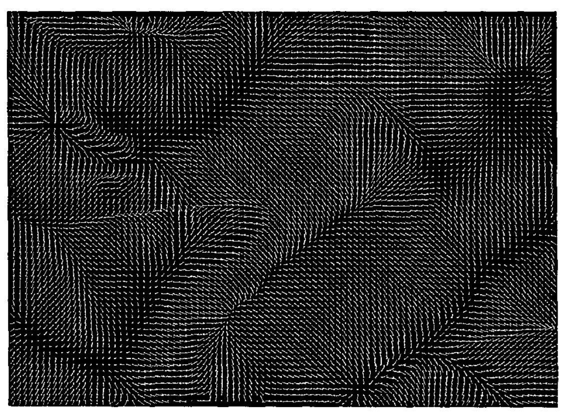

Figure 6. Surface normal vectors smoothed by the surface consistency approach.